On electromagnetic contributions in WIMP quests

R. Bernabei, P. Belli, F. Montecchia, F. Nozzoli
Dip. di Fisica, Università di Roma "Tor Vergata" and INFN, sez. Roma "Tor Vergata", I-00133 Rome, Italy

F. Cappella, A. Incicchitti, D. Prosperi
Dip. di Fisica, Università di Roma "La Sapienza" and INFN, sez. Roma, I-00185 Rome, Italy

R. Cerulli
Laboratori Nazionali del Gran Sasso, INFN, Assergi, Italy

C.J. Dai, H.L. He, H.H. Kuang, J.M. Ma, X.D. Sheng, Z.P. Ye[1]
IHEP, Chinese Academy, P.O. Box 918/3, Beijing 100039, China

Abstract

The effect pointed out by A. B. Migdal in the 40's (hereafter named Migdal effect) has so far been usually neglected in the direct searches for WIMP Dark Matter candidates. This effect consists in the ionization and the excitation of bound atomic electrons induced by the recoiling atomic nucleus. In the present paper the related theoretical arguments are developed and some consequences of the proper accounting for this effect are discussed by some examples of practical interest.

Keywords: Dark Matter; WIMP; underground Physics
PACS numbers: 95.35.+d

1 Introduction

The Migdal effect is known since long time and is described both in devoted papers [1] and in textbooks [2]; it has also been recently addressed for the Dark Matter (DM) field in ref. [3]. This effect consists in the ionization and the excitation of bound atomic electrons induced by the presence of a recoiling atomic nucleus. In this paper, it will be accounted in the case of the WIMP-nucleus elastic scattering. In fact, since the recoiling nucleus can "shake off" some of the atomic electrons, an electromagnetic contribution is present together with a recoil signal in the analysis of DM direct searches (with whatever approach) when interpreted in terms of WIMP candidates. Since this contribution is not quenched, one can expect that this part (usually unaccounted) can play a role as well.

---

[1]also: University of Jing Gangshan, Jiangxi, China

In this paper the related theoretical framework is developed and some of the previous corollary analyses for WIMP candidates [4, 5, 6] from the DAMA/NaI annual modulation results (total exposure of 107731 kg × day) are used for template purpose. We just remind that, in order to investigate in a model independent way the presence of DM particle component(s) in the galactic halo, DAMA/NaI [7, 8, 4, 5] has exploited over seven annual cycles the DM annual modulation signature, achieving a 6.3 σ C.L. model independent evidence [4, 5]. Some of the many possible corollary quests for the candidate particle(s) have also been carried out so far mainly focusing various possibilities for the class of DM candidate particles named WIMPs and for the class of light bosons [4, 5, 9, 6]; other corollary quests are also available in literature, such as e.g. in refs. [10, 11, 12, 13, 14, 15, 16], and many other scenarios can be considered as well.

2 Atomic effects due to nuclear recoils

The possible excitation and ionization of the atom by a recoiling nucleus – induced by a WIMP-nucleus elastic scattering – give rise to a certain quantity of electromagnetic radiation made of the escaping electron and of X-rays and/or Auger electrons arising from the rearrangement of the atomic shells. This radiation is fully contained in a detector of suitable size.

Since the WIMP-nucleus interaction is expected to have a very short range (e.g. being mediated by very heavy particles with mass M), the duration of the collision ($\sim \hbar/M \lesssim 10^{-26}$ s) is negligible with respect to the electron orbit periods and to R_a/V_A, where R_a is the atomic size and V_A is the nucleus velocity after the interaction. Thus, the interaction can be considered as instantaneous and a semiclassical description of the recoil process can be applied following the Migdal approach [1, 2]: the target nucleus is assumed to be at rest for $t < t^*$ and at $t = t^*$ it suddenly acquires the $\vec{V}_A$ velocity because of the interaction. Therefore, after the collision the wave function of the electronic states at $t = t^*$ can be approximated as [2]:

$$\Psi'_i = \left[e^{-i\vec{Q}_A \cdot \sum_\alpha \vec{r}_\alpha} \right] \cdot \Psi_i(\vec{r}_1, \vec{r}_2, ...). \tag{1}$$

In this relation: i) $\Psi_i(\vec{r}_1, \vec{r}_2, ...)$ is their wave function in the rest frame of the nucleus before the interaction; ii) $\vec{r}_\alpha$ is the coordinate vector of the $\alpha - th$ electron; iii) $\vec{Q}_A = m_e \vec{V}_A$ with m_e electron mass.

From eq. (1) the probability P_{fi} to reach the intrinsic state $|\Psi_f >$ starting from an initial state $|\Psi'_i >$ can be written as:

$$P_{fi} = |< \Psi_f|\Psi'_i >|^2 = \left| < \Psi_f|e^{-i\vec{Q}_A \cdot \sum_\alpha \vec{r}_\alpha}|\Psi_i > \right|^2. \tag{2}$$

In the following, the case of the transition of an electron from one level to another and the case of its transition to the continuum (that is, the ionization of the atom) are separately analysed applying the reasonable approximation that multiple transition/ionization processes can safely be neglected.

2.1   Calculation of the excitation probability and profile

The total transition probability can be calculated from the single electron transition probability, P^1_{fi}, by exploiting the mean field approximation. In particular, we consider that the wave function of a single electron does not depend on the coordinates of the other ones. Thus, the probability P^1_{fi} of the transition of a single electron from an initial state $|\psi_i>$ to a final bound state $|\psi_f>$ is simply:

$$P^1_{fi} = \left| < \psi_f | e^{-i\vec{Q}_A\vec{r}} | \psi_i > \right|^2 , \tag{3}$$

where $\vec{r}$ is the coordinate vector of the considered electron.

The term $e^{-i\vec{Q}_A\vec{r}}$ can safely be expanded in series by applying the dipole approximation. In fact, since V_A is at maximum of the order of the impinging WIMP velocity (less than the Galaxy escape velocity: $\sim 2 \cdot 10^{-3} c$) and $R_a \sim 10^{-10}$ m, we can write $\epsilon = Q_A R_a \simeq \frac{m_e V_A R_a}{197 MeV fm} \lesssim 1$. Thus, considering that in practice: $\psi_i(\vec{r}) \sim 0$ for $r > R_a$ and $\vec{Q}_A\vec{r} \leq Q_A r$, the amplitude in eq. (3) can be re-written as:

$$< \psi_f | e^{-i\vec{Q}_A\vec{r}} | \psi_i > \simeq < \psi_f | (1 - i\vec{Q}_A\vec{r} - \tfrac{1}{2}(\vec{Q}_A\vec{r})^2 + ...) | \psi_i > \tag{4}$$

retaining only the leading orders.

As first, the probability for a single electron to retain the same state can be written as:

$$\begin{aligned} P^1_{ii} &= \left| < \psi_i | e^{-i\vec{Q}_A\vec{r}} | \psi_i > \right|^2 = F_i^2 \\ &\simeq \left| < \psi_i | (1 - i\vec{Q}_A\vec{r} - ...) | \psi_i > \right|^2 \sim 1 - O(\epsilon^2) \lesssim 1, \end{aligned} \tag{5}$$

where F_i is the atomic Form Factor of the orbital described by the ψ_i wave function. It can be derived from the Rayleigh scattering database (RTAB) [17], where the atomic Form Factors for the levels of the various atoms are reported. Some examples of the used atomic Form Factors for the Sodium and Iodine atoms are reported in Fig. 1; for the shell 1s the atomic Form Factors calculated by means of the hydrogenic wave functions are also reported for comparison, showing a good agreement.

On the other hand, for the transitions $(f \neq i)$ one gets:

$$P^1_{fi} \simeq \left| < \psi_f | (1 - i\vec{Q}_A\vec{r} - ...) | \psi_i > \right|^2 \simeq \left| < \psi_f | \vec{Q}_A\vec{r} | \psi_i > \right|^2 \sim O(\epsilon^2) \ll 1 \tag{6}$$

because of the states orthogonality.

If we define θ as the angle between the vectors $\vec{Q}_A$ and $\vec{r}_{fi} = < \psi_f | \vec{r} | \psi_i >$, this transition probability can be re-written as:

$$P^1_{fi} \simeq cos^2(\theta) Q_A^2 |r_{fi}|^2 . \tag{7}$$

Since the atoms are unpolarized, $cos^2(\theta)$ can be replaced by its average: 1/3, that is

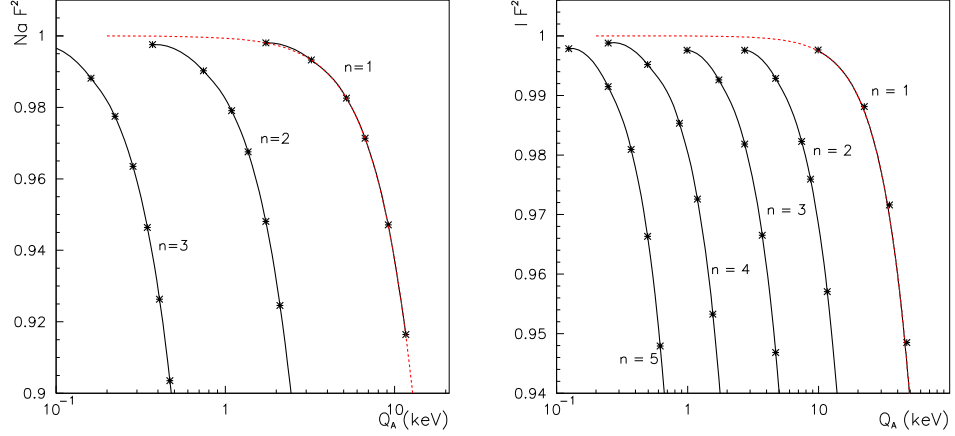$$P^1_{fi} \simeq \frac{1}{3} Q_A^2 |r_{fi}|^2 . \tag{8}$$

Figure 1: Atomic Form Factors from [17] averaged over the shell for various principal quantum numbers of Sodium (left) and Iodine (right) atoms. For the shell 1s the Form Factors calculated by means of the hydrogenic wave functions (dashed lines) are also reported for comparison.

The r_{fi} matrix elements are connected with the standard dimensionless oscillator strengths, f_{fi}, by means of (as usual, here: $\hbar = 1$):

$$f_{fi} = \frac{2m_e\omega_{fi}}{3}|r_{fi}|^2 \tag{9}$$

where ω_{fi} is the energy of the transition and, in conclusion, the transition probability can be expressed as:

$$P^1_{fi} \simeq \frac{Q_A^2 f_{fi}}{2m_e\omega_{fi}} \ . \tag{10}$$

The oscillator strengths for several atoms can also be derived from the Rayleigh scattering database [17]. Some examples of averaged oscillator strengths, calculated on this basis for various atoms, are reported in Table 1 together with some other evaluations available in literature.

Let us now consider the general case. The probability of a single electron in the state i to have a transition to a free bound level (excitation) can be derived by summing over all the available possible states:

$$P^1_{bound,i} \simeq \sum_{j \in free \ bound \ states} | < \psi_j|\vec{Q}_A\vec{r}|\psi_i > |^2, \tag{11}$$

neglecting the probability that other electrons fill the j-th state in the meantime. After an excitation, the atom returns to the ground state emitting X-rays and/or Auger electrons. The total energy released by the process is equal to the transition energy and it depends on the energy level of the final state. Considering that all the

4

Table 1: Some examples of the averaged oscillator strengths – calculated from the Rayleigh scattering database [17] – for various atoms and transitions, together with some other evaluations available in literature.

Atom	Transition	f_{fi} from [17]	f_{fi} from literature
H	$1s \rightarrow 2p$	0.416	0.416 [18]
H	$1s \rightarrow 3p$	0.079	0.079 [18]
H	$1s \rightarrow 4p$	0.029	0.029 [18]
Na	$3s \rightarrow 2p$	-0.042	-0.043 [19]
Na	$3s \rightarrow 3p$	0.968	0.983 [19]
Li	$2s \rightarrow 2p$	0.762	0.753 [19]
K	$4s \rightarrow 4p$	1.045	1.02 [19]

free bound levels are within at maximum few eV, we can safely neglect the spread of the excitation energies. Thus, the excitation profile of the i-th electron can simply be assumed to be a Dirac delta function centered around the average excitation energy, $\langle E \rangle_i$; this is generally less than few eV below the ionization threshold. Therefore, considering the excitations of the single i-th electron, the differential distribution of the electromagnetic part of the detected energy[2], E_{em}, for a given energy, E_0, provided by the WIMP to the nucleus at time t^*, is given by:

$$\frac{dN_{excitation,i}}{dE_{em}}(E_{em}|E_0) = P^1_{bound,i}\delta(E_{em} - \langle E \rangle_i) \,. \tag{12}$$

2.2 Calculation of the ionization probability and profile

The probability of a single electron in the state i to have a transition to the continuum (ionizing the atom), $P^1_{ion,i}$, can be derived as the difference between the unity and the probability of all the other possible processes. They are the following: i) the electron has no transition ($P^1_{ii} = F^2_i$); ii) the electron inter-exchanges the states with another electron ($P^1_{exc,i}$); iii) the electron excites to a free bound level ($P^1_{bound,i}$). Hence:

$$P^1_{ion,i} = 1 - P^1_{ii} - P^1_{exc,i} - P^1_{bound,i} \tag{13}$$

Taking into account the Pauli exclusion principle, the transition to an occupied state j is possible only if the j-th electron goes to another state. Thus, the exchange probability can be estimated by the expression:

$$P^1_{exc,i} \simeq \sum_{j \in occupied\ bound\ states} |<\psi_j|\vec{Q}_A\vec{r}|\psi_i>|^2(1 - F^2_j) \tag{14}$$

having neglected the probability that other electrons fill the j-th state in the meantime.

Unlike the excitation, the differential distribution, $\frac{dN_{ionization,i}}{dE_{em}}$, considering the ionization due to the single i-th electron gives a continuum spectrum:

$$\frac{dN_{ionization,i}}{dE_{em}}(E_{em}|E_0) = P^1_{ion,i}D^i_{ion}(E_{em}) \,, \tag{15}$$

where the ionization profile $D^i_{ion}(E_{em})$ is evaluated in the following (see later).

---

[2]It is the sum of all the energies of the X-rays and Auger electrons, while in case of the ionization process – see later – also the energy of the electron escaping from the atom contributes.

Table 2: Estimated probabilities of excitation and ionization by Migdal effect during a 10 keV kinetic energy Na recoil or during a 33.3 keV kinetic energy I recoil. Although the calculated probabilities are quite small, the unquenched nature of the electromagnetic contribution, the behaviour of the energy distribution for nuclear recoils induced by WIMP-nucleus elastic scatterings, etc. can give an appreciable impact at low WIMP masses; see later.

Atom	Shell	P_{ii}^1	$P_{exc,i}^1$	$P_{bound,i}^1$	$P_{ion,i}^1$	$< E >_i$ (keV)
Na	1s	0.99985	$1.7 \cdot 10^{-7}$	$7.8 \cdot 10^{-7}$	$1.5 \cdot 10^{-4}$	1.062
	2s	0.99595	$1.2 \cdot 10^{-5}$	$2.7 \cdot 10^{-5}$	$4.0 \cdot 10^{-3}$	0.062
	2p	0.99595	$4.1 \cdot 10^{-6}$	$1.5 \cdot 10^{-4}$	$3.9 \cdot 10^{-3}$	0.033
I	1s	0.99999	$2.9 \cdot 10^{-10}$	$2.8 \cdot 10^{-10}$	$3.3 \cdot 10^{-6}$	33.166
	2s	0.99996	$8.4 \cdot 10^{-9}$	$7.3 \cdot 10^{-9}$	$4.5 \cdot 10^{-5}$	5.161
	2p	0.99996	$9.8 \cdot 10^{-9}$	$8.9 \cdot 10^{-9}$	$4.5 \cdot 10^{-5}$	4.687
	3s	0.99966	$1.9 \cdot 10^{-7}$	$1.1 \cdot 10^{-7}$	$3.4 \cdot 10^{-4}$	1.054
	3p	0.99966	$1.8 \cdot 10^{-7}$	$1.5 \cdot 10^{-7}$	$3.4 \cdot 10^{-4}$	0.894
	3d	0.99966	$6.6 \cdot 10^{-8}$	$3.5 \cdot 10^{-8}$	$3.4 \cdot 10^{-4}$	0.635
	4s	0.99730	$5.5 \cdot 10^{-6}$	$1.3 \cdot 10^{-6}$	$2.7 \cdot 10^{-3}$	0.190
	4p	0.99730	$6.8 \cdot 10^{-6}$	$3.8 \cdot 10^{-6}$	$2.7 \cdot 10^{-3}$	0.138
	4d	0.99730	$6.5 \cdot 10^{-6}$	$1.2 \cdot 10^{-5}$	$2.7 \cdot 10^{-3}$	0.058
	5s	0.98102	$2.5 \cdot 10^{-4}$	$2.5 \cdot 10^{-5}$	$1.9 \cdot 10^{-2}$	0.019
	5p	0.98102	$8.5 \cdot 10^{-5}$	$7.3 \cdot 10^{-3}$	$1.2 \cdot 10^{-2}$	0.009

In Table 2 some numerical estimates of the probabilities of the Migdal effect, discussed in the previous and in the present sections, are given. It is worth to note that, although these probabilities are quite small, the electromagnetic unquenched nature of the contribution, the behaviour of the energy distribution for nuclear recoils induced by WIMP-nucleus elastic scatterings, etc. have some impact at low WIMP masses (see later).

Considering the free electron approximation (that is, neglecting the interaction of the escaping electron with the nucleus), the final state of the escaping electron can be described as a plane wave [20]: $\psi_{\vec{p}_f} \simeq \frac{e^{i\vec{p}_f \vec{r}}}{\sqrt{V}}$, normalized to a volume V. The final state density is: $\rho_f = \frac{V d^3 p_f}{(2\pi)^3}$.

Thus, the ionization probability, for an escaping electron with momentum $\vec{p}_f$, can be written as:

$$
\begin{aligned}
dW_{\vec{p}_f i} &= \left| < \psi_{\vec{p}_f} | e^{-i\vec{Q}_A \vec{r}} | \psi_i > \right|^2 \rho_f \simeq \left| \int \frac{e^{-i\vec{p}_f \vec{r}}}{\sqrt{V}} e^{-i\vec{Q}_A \vec{r}} \psi_i(\vec{r}) d^3 r \right|^2 \frac{V d^3 p_f}{(2\pi)^3} \simeq \\
&\simeq \left| \int \frac{e^{-i(\vec{Q}_A + \vec{p}_f)\vec{r}}}{\sqrt{(2\pi)^3}} \psi_i(\vec{r}) d^3 r \right|^2 d^3 p_f = |\phi_i(\vec{p})|^2 d^3 p_f = \rho_i(\vec{p}) d^3 p_f , \quad (16)
\end{aligned}
$$

where: i) $\vec{p} = \vec{p}_f + \vec{Q}_A$; ii) $\phi_i(\vec{p})$ is the wave function of the initial state in the momentum space; iii) $\rho_i(\vec{p})$ is the probability density to find a momentum $\vec{p}$ when the

6

electron is bound with wave function ψ_i. The ionization profile, $\rho_i(\vec{p})$, is normalized to 1, as it can be easily demonstrated: $\int \phi_i^*(\vec{p})\phi_i(\vec{p})d^3p_f = \langle\phi_i|\phi_i\rangle = 1$.

Finally, for practical purposes $Q_A \ll p_f$; in fact, since the maximum energy provided by the WIMP with mass, m_W, and velocity, v, to a nucleus with mass, m_A, is $E_{0,max} = \frac{1}{2}m_W v^2 \frac{4m_W m_A}{(m_W+m_A)^2}$, the maximum velocity is: $V_{A,max} = \frac{2m_W}{m_W+m_A}v \le 2v$. Therefore, $Q_A \ll 3$ keV and can be safely neglected with respect to p_f when the electron energy is larger than 10 eV.

The energy distribution of the escaping electron can be obtained from eq. (16) by introducing the variable $E_f = \frac{p_f^2}{2m_e}$ (escaping energy of the electron) and by integrating over the solid angle. The angular integration can be easily performed by considering an average ionization profile for all the Z_{shell} electrons in a full shell, where $\rho_{shell}(p_f) = \frac{1}{Z_{shell}}\sum_{shell}\rho_i(\vec{p}_f)$ is isotropic. Thus, we can define the ionization profile of a given shell as a function of the escaping energy of the electron according to:

$$D_{ion}^{shell}(E_f) \cdot dE_f \simeq 4\pi m_e \cdot \sqrt{2m_e E_f} \cdot \rho_{shell}(p_f) \cdot dE_f \ , \tag{17}$$

Moreover, in the real cases, the ionization is energetically allowed only for $E_b \le E_f \le E_0$, with E_b binding energy of the electron.
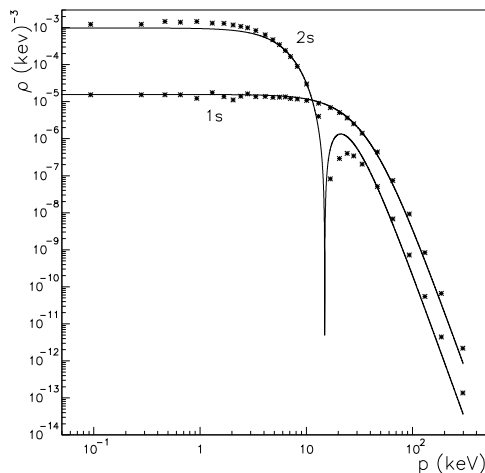

Figure 2: Example of $\rho_{1s}(p)$ and $\rho_{2s}(p)$ for Na atom as extracted from the Compton profile tables [21] by means of the procedure given in the text (stars). The solid lines – shown for comparison – are the $\rho_{1s}(p)$ and $\rho_{2s}(p)$ analytically calculated using hydrogenic wave functions and accounting for the screening effect of the inner electrons ($Z_{eff} = 10$ and $Z_{eff} = 8$ respectively).

In order to obtain the functions $\rho_{shell}(p)$, one can use the tables of the Compton profile $J_i(p_z) = \int \int \rho_i(\vec{p})dp_x dp_y$ available in literature [21] for the various shells of atoms [3]. As examples, $\rho_{1s}(p)$ and $\rho_{2s}(p)$ for Na atom are reported in Fig. 2 as

---

[3]In fact, for isotropic distributions (e.g. for s shell or for full shells) the following relation holds [22, 23]: $J_{shell}(p_z) = \int \int \rho_{shell}(p)dp_x dp_y = 2\pi \int_{p_z}^{\infty} p\rho_{shell}(p)dp$ and, hence: $\rho_{shell}(p) = -\frac{1}{2\pi p}\frac{dJ_{shell}(p)}{dp}$. Thus, the $\rho_{shell}(p)$ values of interest can be evaluated by means of the $J_{shell}(p)$ tables given in ref. [21].

extracted from the Compton profile tables [21]. They show a rather good agreement with the values calculated by using the hydrogenic wave functions and accounting for the screening effect of the inner electrons; these latter ones are also shown in the figure for comparison.

3 Calculation of the expected counting rate

For each given energy, E_0, provided by the WIMP to the nucleus at time t^*, the differential distribution, $\frac{dN_i}{dE_{em}}$, considering the transitions (ionizations/excitations) of the single i-th electron, is given by the sum of the two contributions of eq. (12) and eq. (15). Moreover, the probability density distribution to have an electromagnetic release, E_{em}, for a given E_0 value (considering all the contributions from all the electrons in the atom) can be written as:

$$\frac{dN_{tot}}{dE_{em}}(E_{em}|E_0) \simeq P_{E_0}^0 \delta(E_{em}) + \sum_i \frac{P_{E_0}^0}{P_{i,E_0}^0} \frac{dN_i}{dE_{em}}(E_{em}|E_0) + ... \,, \tag{18}$$

where the term $P_{E_0}^0$ is the probability for the whole atom to remain unchanged: $P_{E_0}^0 \simeq \prod_i P_{i,E_0}^0$, and $P_{i,E_0}^0 = 1 - P_{ion,i}^1 - P_{bound,i}^1$ is the probability that a single electron has no transition either to free bound level or to the continuum. In eq. (18) the expansion can be stopped at the shown level because the probability of multiple excitation/ionization is negligible.

Finally, let us rewrite eq. (18) as a function of the detected energy, E_{det}, which is given by the sum of the recoil detected energy, E_{fr}, and of the electromagnetic component (the relation $\frac{E_{fr}}{q_A} + E_{em} = E_0$ holds):

$$\frac{dN}{dE_{det}}(E_{det}|E_0) = \frac{dN_{tot}}{dE_{em}}(E_{em}|E_0) \cdot \frac{dE_{em}}{dE_{det}} = \frac{1}{1-q_A} \cdot \frac{dN_{tot}}{dE_{em}}(E_{em}|E_0) \,, \tag{19}$$

where q_A is the nuclear recoil quenching factor for the considered nucleus in the given detector at the considered energy.

In particular, let us now point out the case of recoils induced by WIMP-nucleus elastic scatterings under the usual hypothesis that just one component of the dark halo can produce elastic scatterings on nuclei.

For every target specie A, the expected energy distribution including the Migdal effect, $\frac{dR_A^{(M)}}{dE_{det}}(E_{det})$, requires the E_0 differential distribution produced in the WIMP-nucleus elastic scattering, given in squared brackets:

$$\frac{dR_A^{(M)}}{dE_{det}}(E_{det}) = \int \frac{dN}{dE_{det}}(E_{det}|E_0) \left[N_T \frac{\rho_W}{m_W} \int_{v_{min}(E_0)}^{v_{max}} \frac{d\sigma}{dE_0}(v, E_0) v f(v) dv \right] dE_0 \,. \tag{20}$$

There: i) N_T is the number of target nuclei of A specie; ii) $\rho_W = \xi \rho_0$, where ρ_0 is the local halo density and $\xi \leq 1$ is the fractional amount of local WIMP density; iii) $f(v)$ is the WIMP velocity (v) distribution in the Earth frame; iv) $v_{min} = \sqrt{\frac{m_A \cdot E_0}{2m_{WA}^2}}$ (m_{WA} is the reduced mass of the WIMP-nucleus system); v) v_{max} is the maximal WIMP velocity in the halo evaluated in the Earth frame; vi) $\frac{d\sigma}{dE_0}(v, E_0) = \left(\frac{d\sigma}{dE_0}\right)_{SI} + \left(\frac{d\sigma}{dE_0}\right)_{SD}$,

with $\left(\frac{d\sigma}{dE_0}\right)_{SI}$ spin independent (SI) contribution and $\left(\frac{d\sigma}{dE_0}\right)_{SD}$ spin dependent (SD) contribution.

Finally, the expected differential counting rate as a function of the detected energy, E_{det}, for a real multiple-nuclei detector (as e.g. the NaI(Tl)) can be easily derived by summing the eq. (20) over the nuclei species and taking into account the detector energy resolution:

$$\frac{dR^{NaI}}{dE_{det}}(E_{det}) = \int G(E_{det}, E') \sum_{A=Na,I} \frac{dR_A^{(M)}}{dE'}(E')dE' . \tag{21}$$

The $G(E_{det}, E')$ kernel generally has a gaussian behaviour.

Obviously the expected differential counting rate has to be evaluated in given astrophysical, nuclear and particle physics scenarios, also requiring assumptions on all the parameters needed in the calculations and the proper consideration of the related uncertainties (for some discussions see e.g. [4, 5, 6]).
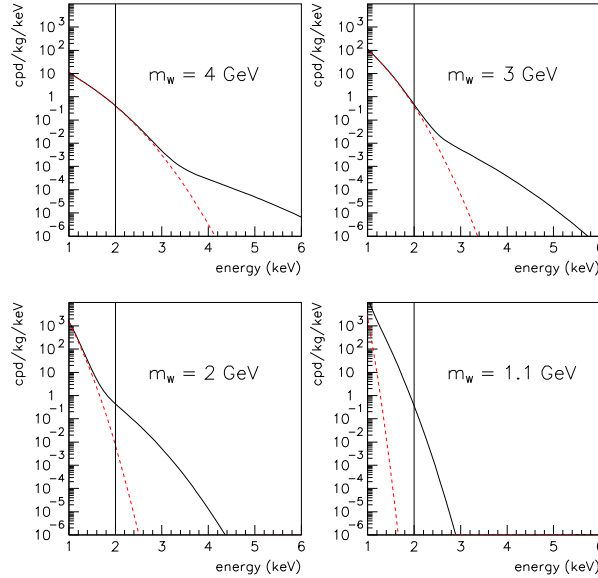

Figure 3: Examples of shapes of expected energy distributions from WIMP-nucleus elastic scatterings in the NaI(Tl) detectors of DAMA/NaI with (continuous line) and without (dashed line) including the Migdal effect, for the model framework given in the text. The effect of the inclusion of this existing physical effect is evident. The vertical lines indicate the DAMA/NaI energy threshold.

For clarity, Fig. 3 shows just few examples of shapes of expected energy distributions with and without accounting for the Migdal effect. For this template purpose – accounting also for the experimental features of the detectors [7, 8, 4, 5] – we just adopt the following assumptions among all the possibilities: i) WIMP with dominant Spin Independent coupling and with nuclear cross sections $\propto A^2$; ii) non-rotating Evans'

logarithmic galactic halo model with core radius $R_c = 5$ kpc, local velocity $v_0 = 170$ km/s and $\rho_0 = 0.42$ GeV cm^{-3} (B1 halo model in ref. [4, 5]); iii) form factors and quenching factors of ^{23}Na and ^{127}I as in case C of ref. [4]. The used normalizations assure the same vertical scale in the shown plots. It is clear the fraction of events at very low WIMP masses of electromagnetic nature. Note that other choices of the model framework do not change the substance of the results.

4   Some examples

The proper accounting of the Migdal effect in corollary quests for WIMPs as DM candidate particles can be investigated by exploiting the expected energy distribution, derived above, to some of the previous analyses on the DAMA/NaI annual modulation data in terms of WIMP-nucleus elastic scattering. For this purpose, the same scaling laws and astrophysical, nuclear and particles physics frameworks of refs. [4, 5] are adopted, while – for simplicity to point out just the impact of the Migdal effect – the SagDEG contribution to the galactic halo, whose effect we discussed in ref. [6], will not be included here.

The results for each kind of interaction are presented in terms of allowed volumes/regions, obtained as superposition of the configurations corresponding to likelihood function values *distant* more than 4σ from the null hypothesis (absence of modulation) in each one of the several (but still a very limited number) of the considered model frameworks. This allows us to account – at some extent – for at least some of the existing theoretical and experimental uncertainties (see e.g. in ref. [4, 5, 9, 6] and in the related astrophysics, nuclear and particle physics literature).

Since the ^{23}Na and ^{127}I are fully sensitive both to SI and to SD interactions, the most general case is defined in a four-dimensional space $(m_W, \xi\sigma_{SI}, \xi\sigma_{SD}, \theta)$, where: i) σ_{SI} is the point-like SI WIMP-nucleon cross section and σ_{SD} is the point-like SD WIMP-nucleon cross section, according to the definitions and scaling laws considered in ref. [4]; ii) $tg\theta$ is the ratio between the effective coupling strengths to neutron and proton for the SD couplings (θ can vary between 0 and π) [4]. The subcase of purely SI coupled WIMPs is shown in Fig. 4, while in Fig. 5 just two slices of the 3-dimensional allowed volume $(m_W, \xi\sigma_{SD}, \theta)$ for the purely SD case are given as an example.

It is worth to note that the accounting for the electromagnetic aspects of the interactions provides in the considered scenarios at the given C.L. additional volumes/regions not topologically connected with the remaining allowed parts. This depends on the behaviour of the expected energy distributions at low masses (where the Migdal contribution is appreciable) with respect to that at higher masses, where recoils dominate.

Finally, in the general case of mixed SI&SD coupling one gets a 4-dimensional allowed volume $(\xi\sigma_{SI}, \xi\sigma_{SD}, m_W, \theta)$; new allowed volume at the given C.L. is present in the GeV region. Fig.6 shows few slices of such a volume as examples.

Note that general comments, extensions and comparisons already discussed in ref. [4, 5, 9, 6] still hold.

Finally, just for completeness, we remind that GeV mass DM particles have been proposed in ref. [24, 25, 26] in order to offer a mechanism able to account for the Baryon Asymmetry in the Universe and to naturally explain why $\Omega_{DM} \sim 5\Omega_b$. Moreover, in
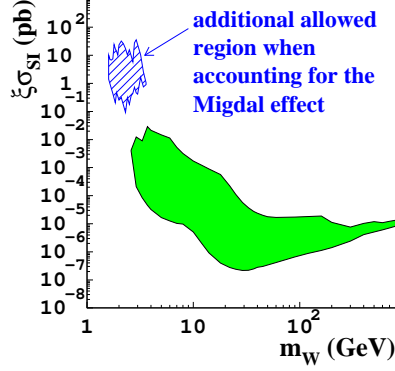
Figure 4: Region allowed in the $(\xi\sigma_{SI}, m_W)$ plane in the considered model frameworks for pure SI coupling; see text. The hatched region appears when accounting for the Migdal effect. Inclusion of other contributions and/or of other uncertainties on parameters and models, such as e.g. the SagDEG contribution [6] or more favourable form factors, would further extend the region and increases the sets of the best fit values. For completeness and more see also [4, 5, 9, 6].
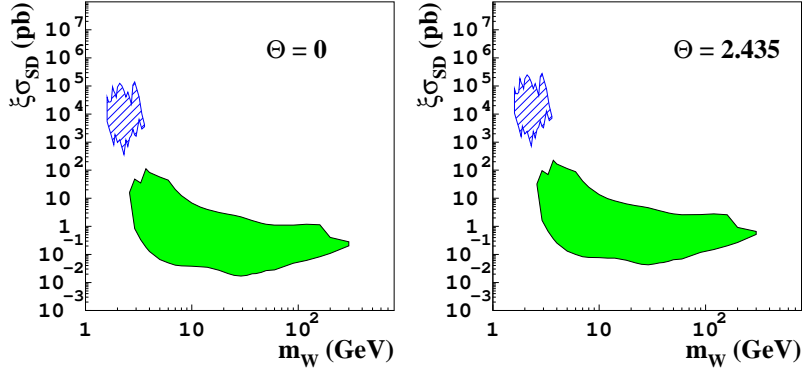

Figure 5: Two slices of the 3-dimensional allowed volume $(\xi\sigma_{SD}, m_W, \theta)$ in the considered model frameworks for pure SD coupling; see text. The hatched regions appear when accounting for the Migdal effect. Analogous remarks as those in the caption of Fig. 4 hold.

ref. [24] it was shown that a GeV mass DM candidate would potentially solve the discrepancies between observations and ΛCDM model on the small scale structure of the Universe. Finally, among the GeV mass WIMP candidates we remind: i) the H dibaryon, already predicted within the Standard Model of particle Physics [26]; ii) the *Darkon*, a real scalar field in an extended Standard Model [27]; iii) the light photino early proposed in models of low-energy supersymmetry [28]; iv) the very light neutralino in Next-to-MSSM model [29]; v) the scalar GeV mass DM candidates of ref. [30]; vi) the mirror Deuterium in frameworks where mirror matter interactions
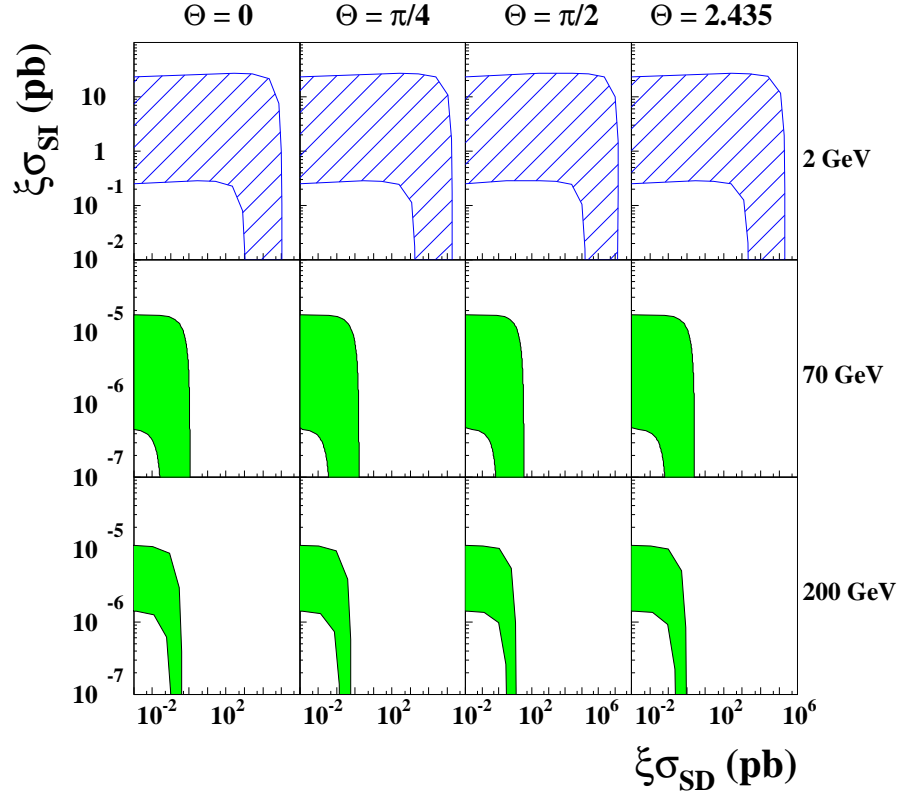
Figure 6: Examples of slices of the 4-dimensional allowed volume $(\xi\sigma_{SI}, \xi\sigma_{SD}, m_W, \theta)$ in the considered model frameworks; see text. The hatched slice appears when accounting for the Migdal effect. Analogous remarks as those in the caption of Fig. 4 hold.

[31] with ordinary matter are dominated by very heavy particles.

5 Conclusions

In this paper the ionization and the excitation of bound atomic electrons induced by the perturbation of the recoiling nucleus after a WIMP elastic scattering have been discussed. This effect has so far usually been neglected in the field. The needed theoretical arguments have been developed and the related impact in corollary quests for the candidate particle has been shown, as example, for some simplified scenarios. Obviously, many other arguments can be addressed as well both on DM candidate particles and on astrophysical, nuclear and particle physics aspects; for more see [4, 5, 9, 6] and in literature.

References

[1] A. B. Migdal, J. Phys. USSR 4 (1941) 449; G. Baur, F. Rösel and D. Trautmann, J. Phys. B: At. Mol. Phys. 16 (1983) L419.

[2] A. B. Migdal *Qualitative Methods in Quantum Mechanics* 1977 (Reading, Mass: Benjamin) p. 108; L. D. Landau and E. M. Lifshits *Quantum Mechanics, Non-Relativistic Theory* 1977 (Pergamon press), 3rd Ed., p. 149.

[3] J.D. Vergados, H. Ejiri, Phys. Lett. B 606 (2005) 313; Ch.C. Moustakidis, J.D. Vergados, H. Ejiri, Nucl. Phys. B 727 (2005) 406; H. Ejiri, Ch.C. Moustakidis, J.D. Vergados, Phys. Lett. B 639 (2006) 218.

[4] R. Bernabei el al., La Rivista del Nuovo Cimento 26 n.1 (2003) 1-73.

[5] R. Bernabei el al., Int. J. Mod. Phys. D 13 (2004) 2127.

[6] R. Bernabei et al., Eur. Phys. J. C. 47 (2006) 263.

[7] R. Bernabei et al., Il Nuovo Cim. A 112 (1999) 545.

[8] R. Bernabei et al., Eur. Phys. J. C 18 (2000) 283.

[9] R. Bernabei et al., Int. J. Mod. Phys. A 21 (2006) 1445.

[10] A. Bottino et al., *Phys. Rev.* D 67 (2003) 063519 ; A. Bottino et al., *Phys. Rev.* D 68 (2003) 043506 .

[11] A. Bottino et al., *Phys. Rev.* D 69 (2004) 037302 .

[12] A. Bottino et al., *Phys. Lett.* B 402 (1997) 113 ; *Phys. Lett.* B 423 (1998) 109 ; *Phys. Rev.* D 59 (1999) 095004 ; *Phys. Rev.* D 59 (1999) 095003 ; *Astrop. Phys.* 10 (1999) 203 ; *Astrop. Phys.* 13 (2000) 215 ; *Phys. Rev.* D 62 (2000) 056006 ; *Phys. Rev.* D 63 (2001) 125003 ; *Nucl. Phys. B* **608** (2001) 461.

[13] K. Belotsky, D. Fargion, M. Khlopov and R.V. Konoplich, hep-ph/0411093.

[14] D. Smith and N. Weiner, Phys. Rev. D 64 (2001) 043502; D. Smith and N. Weiner, Phys. Rev. D 72 (2005) 063509.

[15] R. Foot, hep-ph/0308254.

[16] S. Mitra, Phys. Rev. D 71 (2005) 121302.

[17] L. Kissel, Rad. Phys. and Chem. 59 (2000) 185.

[18] B.H. Brandsen and C.J. Joachain, *Physics of Atoms and Molecules*, Longman group Lim, London 1983.

[19] P.H. Heckmann and E. Trabert, *Introduction to the spectroscopy of atoms*, North-Holland 1989.

[20] J. Als-Nielsen and D. McMorrow, *Elements of Modern X-ray Physics*, J. Wiley & Sons, Ltd. 2001.

[21] F. Biggs et al., Atomic data and nuclear data tables 16 (1975) 201.

[22] D. Brusa et al., Nucl. Inst. & Meth. A 379 (1996) 167.

[23] R. Ribberford et al., Phys. Rev. A 26 (1982) 3325; Phys. Rev. B 12 (1975) 2067.

[24] R. Kitano and I. Low, Phys. Rev. D 71 (2005) 023510.

[25] N. Cosme, L.L. Honorez and M.H.G. Tytgat, Phys. Rev. D 72 (2005) 043505.

[26] G. Farrar and G. Zaharijas, Phys. Rev. Lett. 96 (2006) 041302; G. Zaharijas and G. Farrar, Phys. Rev. D 72 (2005) 083502; G. Zaharijas astro-ph/0510088.

[27] X.G. He et al., hep-ph/0701156.

[28] D.J.H. Chung, G.R. Farrar, E.W. Kolb, Phys. Rev. D 56 (1997) 6096; G.R. Farrar, E.W. Kolb, Phys. Rev. D 53 (1996) 2990.

[29] J.F. Gunion, D. Hooper, B. McElrath, Phys. Rev. D 73 (2006) 015011.

[30] C. Bœhm and P. Fayet, Nucl. Phys. B 863 (2004) 219.

[31] Z. Berezhiani, Int. J. Mod. Phys. A 19 (2004) 3775.